Protein Nanopores

DOI: 10.1002/anie.201400400

Control of the Conductance of Engineered Protein Nanopores through Concerted Loop Motions**

*Tiandi Zhuang and Lukas K. Tamm**

Abstract: *Protein nanopores have attracted much interest for nucleic acid sequencing, chemical sensing, and protein folding at the single molecule level. The outer membrane protein OmpG from E. coli stands out because it forms a nanopore from a single polypeptide chain. This property allows the separate engineering of each of the seven extracellular loops that control access to the pore. The longest of these loops, loop 6, has been recognized as the main gating loop that closes the pore at low pH values and opens it at high pH values. A method was devised to pin each of the loops to the embedding membrane and measure the single-pore conductances of the resulting constructs. The electrophysiological and complementary NMR measurements show that the pinning of individual loops alters the structure and dynamics of neighboring and distant loops in a correlated fashion. Pinning loop 6 generates a constitutively open pore and patterns of concerted loop motions control access to the OmpG nanopore.*

Engineered protein nanopores have attracted interest for the detection of rare metal ions and neurotransmitters in solution,[1] low-cost sequencing of small numbers of molecules of DNA and RNA,[2] and measurement of the folding and unfolding kinetics of single proteins.[3] In most of these studies, engineered versions of the heptameric α-hemolysin nanopore were used, although other proteins have also been used.[4] Single-molecule detection in these systems has been mostly achieved through electrophysiological experiments with nanopores that were reconstituted into planar lipid bilayers. As an alternative, optical detection schemes have also been devised.[5] Although α-hemolysin has been so successful in these studies, a major limitation is its heptameric seven-fold symmetric structure[6], which necessitates the assembly and purification of heteroheptamers. The *E. coli* outer membrane protein OmpG offers an attractive alternative because its nanopore is formed from a single polypeptide chain that folds into lipid bilayers as a 14-stranded β-barrel.[7] Pore access is controlled by seven extracellular loops that have been shown to be highly dynamic and regulated by pH.[8] Despite the promise of OmpG for further nanopore engineering, a drawback has been its loop dynamics, which give rise to flickering single channel currents. This problem has been overcome partially by the engineering of the so-called quiet OmpG mutant, in which strands 12 and 13 were disulfide cross-linked and the irregularly positioned Asp215 in strand 11 was deleted.[9] In the present work, we have devised a new strategy for producing "quiet" OmpG by pinning the loops to the membrane through long-hydrocarbon-chain alkylation (Figure 1 A). Moreover, we have used NMR spectroscopy in lipid micelles to characterize the changes in loop structure and dynamics as a consequence of pinning each of the seven loops. Dodecylation of loop 6 had the largest effect, permanently opening the channel, but other loops are shown to also contribute to channel closing to various degrees and in cooperation with loop 6. Neighboring loops are particularly affected by the pinning of individual loops and loops 1 and 5 were found to cooperate synergistically to control access to the nanopore.

To immobilize individual loops of OmpG and pin them to the membrane, we engineered single cysteine residues into each of the loops. The following sites were chosen to preserve the predominantly negative charge characters of each of the loops, which we figured might be important for their function: Y22C (L1), S58C (L2), E101C (L3), L141C (L4), S182C (L5), I226C (L6), and S266C (L7; Figure 1 B). The introduction of these mutations caused little or no structure perturbation as monitored by ^{1}H,^{15}N-TROSY NMR of OmpG in dodecylphosphocholine (DPC) micelles (data not shown). However, dodecylation of the cysteine residues caused major shifts and broadening of the cross-peaks of nearby residues as exemplified by Ile226 in loop 6 (Figure S1 in the Supporting Information). Residues forming the β-barrel pore structure were not significantly changed by the dodecylation and resulting pinning of the loops to the lipid surface. For simplicity, we call the dodecylated pinned loop mutants of OmpG pL1, pL2, … pL7, for the seven respective loop mutants.

Figure 2 shows a comparison of typical single-channel current traces of wild-type OmpG (wt) and pL6 OmpG flickering between open and closed states at pH 6.0, that is, the pH value that gives equal populations of the two states in the wt.[10] Single-channel activities (10–20 s recording time for each condition) were analyzed in terms of open current, open probability, and closing rate. Gaussian fits of the open probability histograms reveal that wt OmpG was open 62% of the time but pL6 was open nearly 100% of the time. The

[*] Dr. T. Zhuang, Prof. L. K. Tamm
Department of Molecular Physiology and Biological Physics and Center for Membrane Biology
University of Virginia School of Medicine
P.O. Box 800886, Charlottesville, VA 22908 (USA)
E-mail: Lkt2e@virginia.edu
Homepage: http://tammlab.medicine.virginia.edu/

[**] This work was funded by grant R01 GM51329 from the National Institutes of Health. We thank Dr. Binyong Liang and Dr. Hagan Bayley for critically reading the manuscript. L.K.T. would also like to thank Dr. Bayley for his hospitality when this manuscript was written during a sabbatical stay in his laboratory at the University of Oxford.

Supporting information (including experimental details) for this article is available on the WWW under http://dx.doi.org/10.1002/anie.201400400.

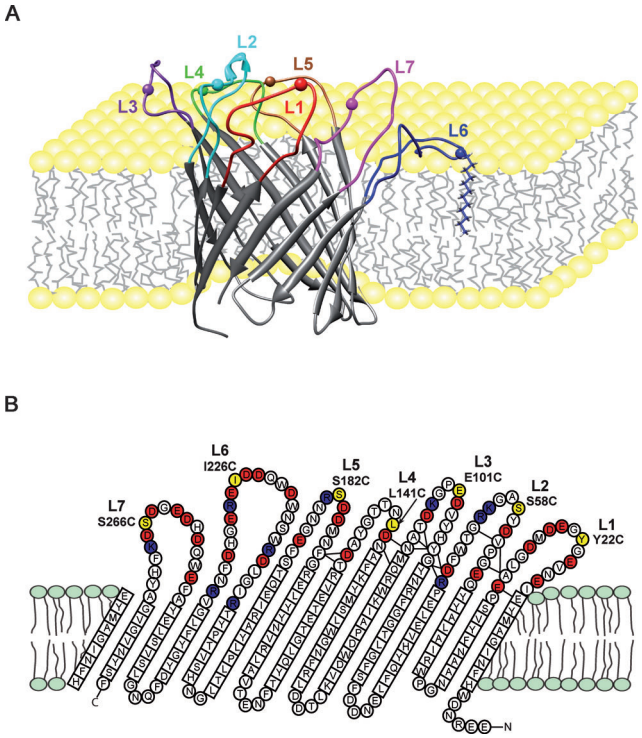

Figure 1. Pinning of loops of the OmpG nanopore to the membrane through dodecylation of engineered cysteines. A) A conformer of the ensemble of solution structures of OmpG[8b] is shown with loop 6 pinned to the membrane by dodecylation at Cys226 (pinned L6, mutant I226C). Similar constructs were made for pinned L1 (mutant Y22C), pinned L2 (mutant S58C), pinned L3 (mutant E101C), pinned L4 (mutant L141C), pinned L5 (mutant S182C), and pinned L7 (mutant S266C). The spheres represent the single cysteine sites. B) The topology of OmpG determined from the solution NMR structure (PDB code 2JQY). 14 transmembrane β-strands are connected by 7 extracellular loops with an excess of negatively charged residues (red) over positively charged residues (dark blue). The residues that were changed to single cysteine residues for alkylation are shown in yellow in each loop.

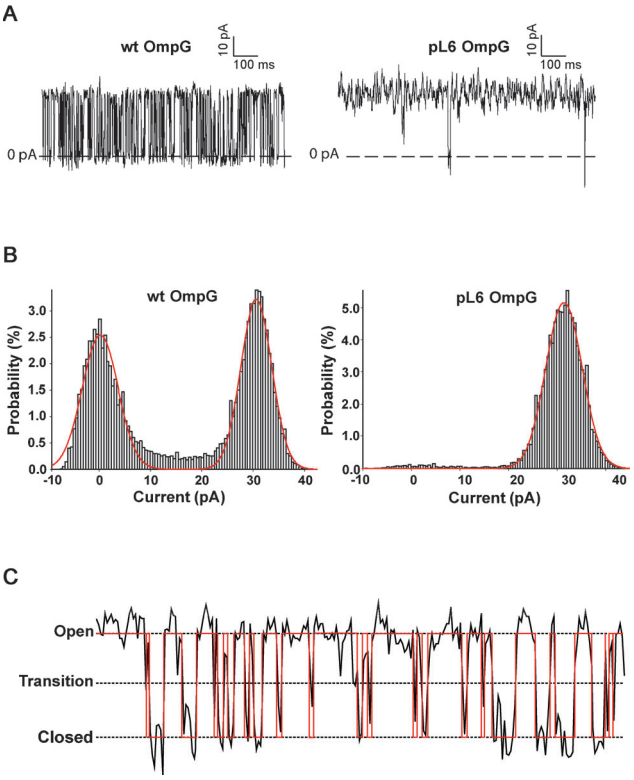

Figure 2. Examples of single-channel current recordings and definition of their open–closed state transitions. A) Typical current recordings of wild-type and pL6 OmpG nanopores at pH 6.0. The insets indicate scale each axis. B) Current histograms of wild-type and pL6 OmpG recordings. The red curves are fits of the data to Gaussian distributions. C) Definition of state transitions. Nanopores are considered open/closed when current > 50%/ < 50% of the open current. The open probability is defined as the fraction of the total recording time that the pore is open. The closing rate is defined as the number of closings per second. The red trace is the binary analysis of the experimental recording.

open currents at 50 mV and 1M KCl were 31 and 33 pA for wt and pL6, respectively, and the closing rate of the wt was 113 s^{-1}. Pinning loops 2, 3, 4, and 6 did not significantly change the open currents of OmpG, but the open currents of pL1 and pL5 were reduced to 19 and 23 pA, respectively (Figure 3). Similarly, the open probabilities of pL1, pL3, and pL5 were not changed much, but pL2, pL4, and pL7 were significantly more open than the wt. Aside from pL6, which was always open, the closing rates of pL2, pL3, and pL7 were the most reduced. Since pL1 and pL5 produced the largest current reductions, we also prepared the double-pinned mutant pL1/5. Interestingly, the open current and open probability of this mutant surpassed that of the wt (Figure 3), thus strongly suggesting that loops 1 and 5 cooperate with each other and likely also with loop 6 in closing the OmpG channel. Only when both loops were immobilized, the channel became 75% open. This double mutant is presumably closed only by the sole remaining major pore-gating loop, loop 6.

The electrophysiological results suggest that loops 1 and 5 can partially substitute for each other and cooperate with loop 6 in closing the OmpG nanopore. Previous NMR ensemble calculations already suggested that some loop conformational changes are correlated.[8b] To more directly demonstrate structural cross-talk between different loops, we recorded ^{1}H,^{15}N-TROSY NMR spectra of each of the single-pinned loop constructs of OmpG and compared the combined ^{1}H-^{15}N chemical shifts to those of the corresponding unreacted free Cys mutant proteins. The chemical shift perturbations show that the pinned loops mostly affect the structures of the neighboring loops (Figure 4). For example, pL3 mostly affects the chemical shifts of loops 2 and 4 (Figure 4C), pL2 affects loops 1 and 3 (Figure 4B), and pL6 affects loops 5 and 7 (Figure 4F). Some other pinned-loop perturbations reach further to the second nearest neighbors. For example, pL1 affects the structures of loops 6, 7, and 2 (Figure 4A) and pL4 affects the structures of loops 2, 3, and 5 (Figure 4D). pL5 is the only exception: in addition to affecting the neighboring loops 4 and 6, it also reaches across and affects the structure of loop 1 (Figure 4E). This structural evidence nicely supports the synergistic effect of

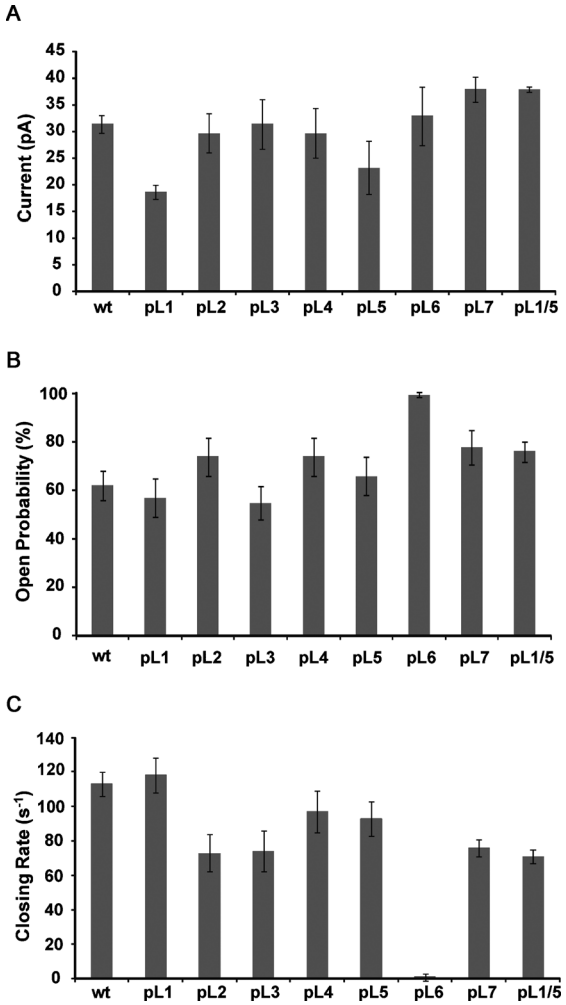

Figure 3. Pinning individual loops changes the electrophysiological activity of the OmpG nanopore. Changes in the the open current (A), open probability (B), and closing rate (C) upon pinning loops 1 through 7 to the membrane by dodecylation are shown. Data for the double-pinned mutant pL1/5 are also shown. All values are averages of at least five independent lipid bilayer measurements.

loops 1 and 5 that we observed electrophysiologically. In summary, the loops of OmpG communicate with each other structurally and undergo concerted structural changes that all contribute to the electrophysiological behavior of the OmpG nanopore. The coupling between the motions of neighboring loops is stronger than distant coupling across the pore, although the latter does occur in the case of the structural cooperation between loops 1 and 5.

If the threshold for structural perturbation is set somewhat lower than the current line at 0.08 ppm in Figure 4, one also finds that pL1 and pL5 affect more loops than the other pL mutants, thus suggesting that L1 and L5 may play a role in scaffolding the other loops. This possible structural scaffold function of loops 1 and 5 could explain the synergism in opening pore access that we observed electrophysiologically.

To examine how pinning affects the motions of the different loops, we measured ^{15}N NMR transverse relaxation times (T_2) of the pL6 mutant D224C before and after dodecylation. Amide ^{15}N T_2 values are inversely proportional to and report on segmental ns timescale correlation times (τ_c) of the polypeptide backbone. A comparison of the T_2 values of the unreacted and dodecylated D224C mutant shows that the segmental motions of most loops on the ns timescale are not significantly affected by the pinning of loop 6 (Figure 5A). However, the pinning of loop 6 at residue 224 resulted in a significant decrease of the T_2 value of nearby Ile226 from 47 to 25 ms. This corresponds to an estimated increase of the segmental loop τ_c from 12 to 28 ns when this loop becomes partially immobilized on the lipid surface.

To assess the stability of dodecyl chain insertion into the membrane, we monitored the accessibility of the disulfide bond by using dithiothreitol (DTT) in DPC micelles and dimyristoylphosphatidylcholine (DMPC) liposomes (Figure S2). I226C was labeled through a disulfide bond with either a nitroxide or a dodecyl chain. Nitroxide-labeled I226C was readily cleaved by DTT, thus suggesting exposure to solvent as expected. Dodecylated I226C was completely protected from disulfide reduction and cleavage by DTT, thus strongly suggesting its burial in DPC micelles and DMPC bilayers. There are previous reports that acyl chains of lipidated peptides and proteins are inserted into lipid model membranes[11] and anchoring of the loops at their two ends to the β-barrel should enhance this interaction. Together with the reduced mobilities of these loops as measured by NMR spectroscopy, these experiments provide strong support for the notion that the lipidated loops are indeed pinned to the membrane.

The opening and closing of the OmpG nanopore by the main gating loop, loop 6, occurs on the low ms timescale (Figure 3C). This and faster timescales can be accessed by NMR relaxation dispersion experiments. We performed ^{15}N Carr-Purcell-Meiboom-Gill (CPMG) relaxation dispersion experiments to probe sub-ms motions of selected loop 6 residues before and after pinning of the neighboring loop 7 and the more distant loop 2 (Figure 5B). The relaxation profiles show exchange rates of ca. 2050 and 2300 s^{-1} for the loop 6 residues Asp225 and Ile226, respectively. When loop 2 was pinned, the exchange rates of the loop 6 residues increased to almost 10000 s^{-1}. However, when loop 7 was pinned, the exchange rate of Asp225 decreased to ca. 1000 s^{-1} and that of Ile226 increased to ca. 5500 s^{-1}. An increase of exchange rates upon pinning of neighboring or more distant loops may be rationalized by restraint of the motions of other loops (loops 2 and 7 in this case) on the sub-ms timescale that would otherwise hinder loop 6 motions. The increase in motional frequency of loop 6 does not imply anything about the open probabilities, which happen to be slightly increased in pL2 and pL7 (Figure 3B). The closing rate is slightly decreased on the ms timescale for pL2 and pL7 (Figure 3C), whereas the increased exchange rates measured by NMR spectroscopy occur on the sub-ms timescale and could reflect opening rates. The reduced exchange rate of Asp225 in pL7 is more difficult to explain and probably reflects some more complex motions of this charged residue when surrounded by the many other charged loop residues (see Figure 1B).

Our new approach of loop immobilization has revealed patterns of cross-talk between different loops in controlling access to the OmpG nanopore. As expected from previous

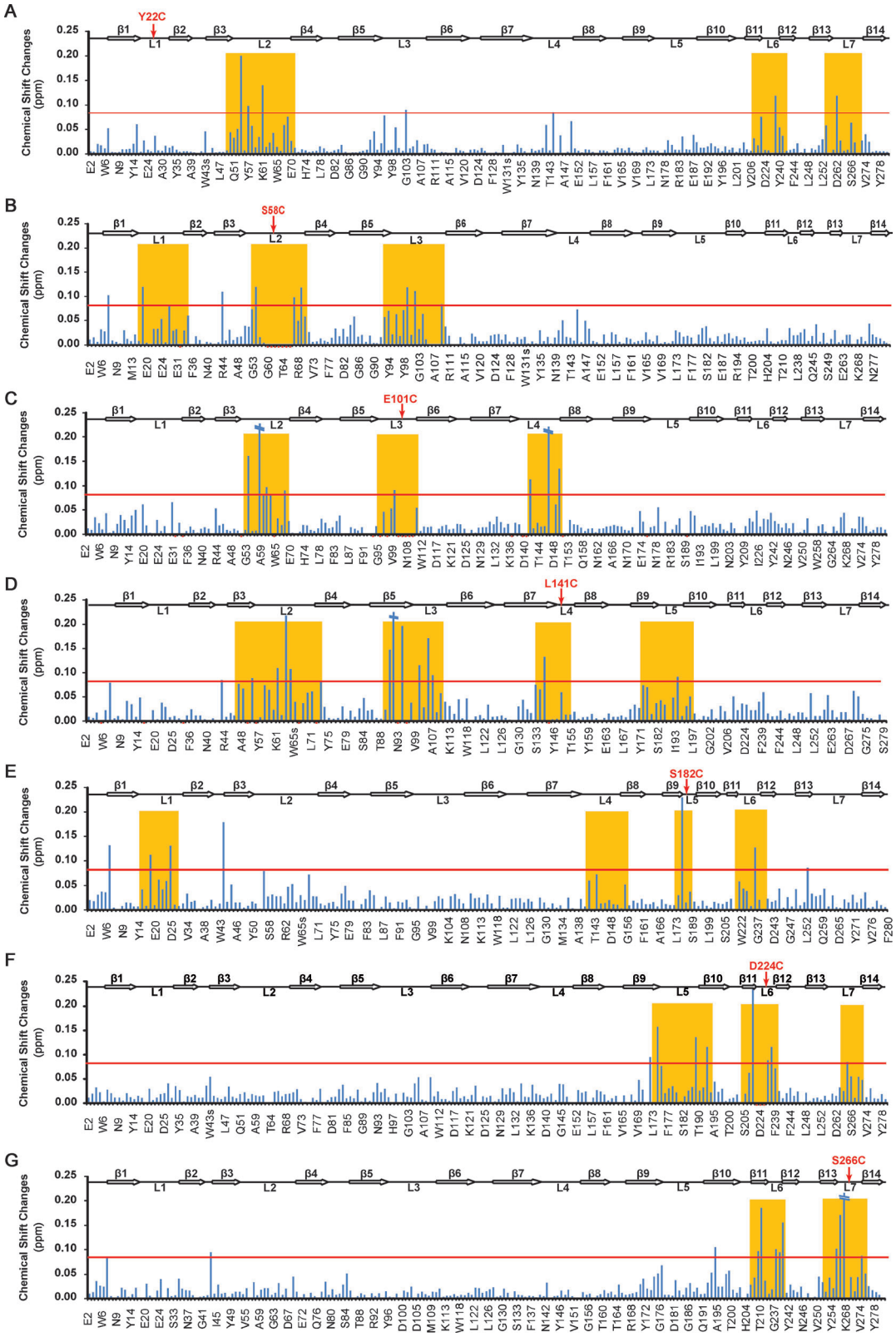

Figure 4. NMR chemical-shift perturbations suggest concerted motions of extracellular loops in pinned OmpG loop mutants. Chemical shift changes between dodecylated OmpG mutants and their unreacted counterparts are plotted for all seven pL mutants. A red line is drawn at 0.08 ppm, which is twice the estimated average measuring error. Chemical shifts were obtained from $^{1}H,^{15}N$-TROSY spectra of ca. 0.5 mM $^{2}H,^{15}N$-labeled protein samples in 150 mM DPC micelles at pH 7.0 and 600 MHz proton frequency.

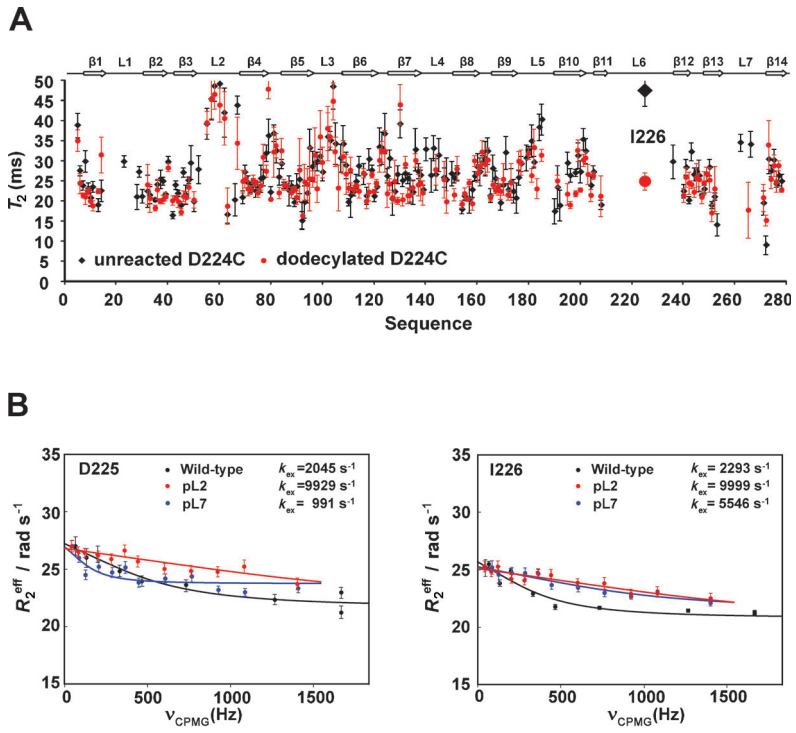

Figure 5. Nanosecond and sub-millisecond dynamics of pinned and unpinned loops of the OmpG nanopore. A) ^{15}N NMR transverse relaxation times (T_2) of ^{2}H,^{15}N-labeled D224C-OmpG unreacted (black) or reacted (red) with a dodecyl chain. The T_2 values were obtained by fitting the relaxation profiles using exponential decays. Error bars represent the fitting errors. Only residues with T_2 values of 0–50 ms are displayed. B) NMR relaxation dispersion experiments indicating correlated sub-millisecond loop motions. ^{15}N CPMG dispersion profiles of Asp225 (left) and Ile226 (right) of wild-type (black), pL2 (red), and pL7 (blue) OmpG. The relaxation dispersion profiles were fitted by a two-state fast exchange model and the resulting exchange rates are indicated in each panel. All data were acquired with ca. 0.5 mM protein samples in DPC micelles at pH 7.0, 800 MHz and 40 °C. k_{ex} = exchange rate, R_2^{eff} = effective transverse relaxation rate.

studies,[7a,8b,12] loop 6 performs the major gating function. When it was pinned to the membrane, a constitutively open pore was found with properties quite similar to those of quietOmpG (Figure S3).[9] pL6 OmpG should therefore be a promising candidate for further nanopore engineering and future practical applications in chemical sensing or sequencing. Structural, dynamics, and functional analysis also revealed important new roles of the other loops of OmpG. For example, we discovered concerted conformational shifts of loops 1 and 5, which may form a scaffold coordinating the conformations of the other loops. Besides the cooperation of loops 1 and 5, any loop affects the conformation of its next and second next neighboring loops. Collective structural changes of the loops have been described before by NMR paramagnetic relaxation enhancement data and derived structural ensemble calculations,[8b] but the current study assigns specific patterns of ordered changes to each of the loops, which may be driven by the high (negative) charge density in the extracellular loops and hydrogen-bonding networks at the bases of the loops (Figure 1B). Conformational loop dynamics have not been described in this much detail for any other porin. Our approach relies on the immobilization of the flexible loops, which can usually be predicted from the amino-acid sequence without prior knowledge of the three-dimensional structure. Therefore, we expect the approach to be general and useful for analyzing the structures and functions of other membrane pores and to guide OmpG nanopore engineering for a range of future practical applications.

Experimental Section

Mutagenesis was performed and proteins were prepared as previously described.[8b] Samples were refolded in octyl β-glucoside and transferred into DPC. Refolded single Cys mutants were reacted with a 10-fold excess of dodecyl methanethiosulfonate (Toronto Research Chemicals, Toronto, CA) overnight and purified by Superdex 200 size-exclusion chromatography. Completeness of dodecylation was confirmed by MALDI-TOF mass spectrometry and NMR. Electrophysiological recordings were obtained at room temperature and an applied voltage of 50 mV as previously described.[8a] Symmetric buffer conditions with Bis-Tris (25 mM) pH 6.0, KCl (1 M) in both chambers were used. ^{1}H,^{15}N-TROSY NMR spectra, T_2 relaxation time, and CPMG relaxation dispersion experiments of ca. 0.5 mM ^{2}H,^{15}N-labeled protein samples in 150 mM DPC micelles were obtained at 40 °C on Bruker Avance 600 or 800 MHz spectrometers in HEPES (25 mM) pH 7.0, NaCl (50 mM), EDTA (0.1 mM), NaN_3 (0.05 %). The unreacted single Cys mutant proteins also contained 5 mM DTT. Bis-Tris = 2,2-bis(hydroxyethyl)iminotris(hydroxymethyl)methane, HEPES = *N*-2-hydroxyethylpiperazine-*N*′-2-ethanesulfonic acid, EDTA = ethylendiaminetetraacetate.

Received: January 14, 2014
Revised: March 12, 2014
Published online: April 28, 2014

Keywords: electrophysiology · NMR spectroscopy · porins · protein engineering · protein nanopores

[1] a) L. S. Choi, T. Mach, H. Bayley, *Biophys. J.* **2013**, *105*, 356–384; b) A. J. Boersma, K. L. Brain, H. Bayley, *ACS Nano* **2012**, *6*, 5304–5308.
[2] a) D. Stoddart, A. J. Heron, E. Mikhailova, G. Maglia, H. Bayley, *Proc. Natl. Acad. Sci. USA* **2009**, *106*, 7702–7707; b) M. Ayub, S. W. Hardwick, B. F. Luisi, H. Bayley, *Nano Lett.* **2013**, *13*, 6144–6150.
[3] D. Rodriguez-Larrea, H. Bayley, *Nat. Nanotechnol.* **2013**, *8*, 288–295.
[4] E. A. Manrao, I. M. Derrington, A. H. Laszlo, K. W. Langford, M. K. Hopper, N. Gillgren, M. Pavlenok, M. Niederweis, J. H. Gundlach, *Nat. Biotechnol.* **2012**, *30*, 349–353.
[5] A. J. Heron, J. R. Thompson, B. Cronin, H. Bayley, M. I. Wallace, *J. Am. Chem. Soc.* **2009**, *131*, 1652–1653.
[6] L. Z. Song, M. R. Hobaugh, C. Shustak, S. Cheley, H. Bayley, J. E. Gouaux, *Science* **1996**, *274*, 1859–1866.
[7] a) O. Yildiz, K. R. Vinothkumar, P. Goswami, W. Kuhlbrandt, *EMBO J.* **2006**, *25*, 5240–5240; b) G. V. Subbarao, B. van den Berg, *J. Mol. Biol.* **2006**, *360*, 750–759.

[8] a) B. Y. Liang, L. K. Tamm, *Proc. Natl. Acad. Sci. USA* **2007**, *104*, 16140 – 16145; b) T. D. Zhuang, C. Chisholm, M. Chen, L. K. Tamm, *J. Am. Chem. Soc.* **2013**, *135*, 15101 – 15113.
[9] M. Chen, S. Khalid, M. S. P. Sansom, H. Bayley, *Proc. Natl. Acad. Sci. USA* **2008**, *105*, 6272 – 6277.
[10] S. Conlan, Y. Zhang, S. Cheley, H. Bayley, *Biochemistry* **2000**, *39*, 11845 – 11854.
[11] L. Brunsveld, H. Waldmann, D. Huster, *Biochim. Biophys. Acta Biomembr.* **2009**, *1788*, 273 – 288.
[12] a) M. Damaghi, C. Bippes, S. Koster, O. Yildiz, S. A. Mari, W. Kuhlbrandt, D. J. Muller, *J. Mol. Biol.* **2010**, *397*, 878 – 882; b) M. Damaghi, S. Koster, C. A. Bippes, O. Yildiz, D. J. Muller, *Angew. Chem.* **2011**, *123*, 7560 – 7562; *Angew. Chem. Int. Ed.* **2011**, *50*, 7422 – 7424.

